

XMM-NEWTON OBSERVATIONS OF THE *LOCKMAN HOLE*: SPECTRA AND TIME VARIABILITY OF THE BRIGHTEST AGN

Mateos S.^{1,2}, Barcons X.², Carrera F.J.², Ceballos M.T.², Hasinger G.³, Lehmann I.³, Streblyanska A.³, and Fabian A.⁴

¹Department of Physics and Astronomy, Leicester University, Leicester LE1 7RH, UK

²Instituto de Física de Cantabria (CSIC-UC), 39005 Santander, Spain

³Max-Planck-Institut für Extraterrestrische Physik, Giessenbachstrasse, Garching D-85748, Germany.

⁴Institute of Astronomy, University of Cambridge, Madingley Road, Cambridge CB3 0HA, UK.

ABSTRACT

We discuss here the main results of a study of the X-ray spectral and variability properties of the 123 brightest objects detected with *XMM-Newton* in the *Lockman Hole* field. This is the deepest observation carried out so far with *XMM-Newton*, with more than 600 ksec of EPIC pn data. Thanks to the good signal to noise of the data (all spectra have more than 500 background subtracted counts) we have been able to put strong constraints on the properties of the X-ray emission of faint Active Galactic Nuclei and on their dependence on luminosity and redshift. To complement the X-ray spectral analysis we carried out a study of the X-ray variability of the same sample of objects on long time scales ranging from days to years.

Key words: X-rays: general, X-ray surveys, galaxies: active.

1. INTRODUCTION

Recent *Chandra* and *XMM-Newton* deep surveys have proven that the Cosmic X-ray background (XRB) at energies above ~ 0.2 keV is made up of the integrated emission of point sources, most being faint Active Galactic Nuclei (AGN). In order to gain insight into the nature and cosmic evolution of the population of AGN, spectral analyses of large samples of objects detected in medium and deep X-ray surveys are being conducted. However the majority of the sources detected in these observations are too faint to provide good spectral information and in many cases some assumptions need to be made prior to the analysis (frequently on the slope of the broad band continuum shape).

With the aim of constrain better the X-ray spectral and variability properties of faint AGN and their dependence

on luminosity and redshift we have carried out a detailed study of the X-ray emission properties of the brightest sources detected with *XMM-Newton* in the *Lockman Hole* field.

Throughout this paper we have adopted the *WMAP* derived cosmology with $H_0 = 70 \text{ km s}^{-1} \text{ Mpc}^{-1}$, $\Omega_M = 0.3$ and $\Omega_\Lambda = 0.7$.

2. THE X-RAY DATA

The *XMM-Newton* deep survey of the *Lockman Hole* is composed of 17 observations carried out from 2000 to 2002. In total we have more than 600 ksec of clean¹ pn data and more than 800 ksec of MOS1 and MOS2 data. A detailed description of how the source list of the total observation was built can be found in Mateos (2005). A total of 268 sources were detected by *XMM-Newton* in the *Lockman Hole*. From this sample we selected the 123 brightest objects (all spectra have more than 500 background subtracted counts) for our analysis. As we are primarily interested in studying the properties of AGN we excluded from the sample sources already identified as clusters of galaxies or stars. At the time of this analysis we had optical spectroscopic identifications available for 74 ($\sim 60\%$) objects, 46 being identified as type-1 AGN and 28 as type-2 AGN.

3. SPECTRAL ANALYSIS

We extracted spectral products, source and background spectra and the corresponding calibration matrices, for each individual observation. The data was then combined to obtain a MOS and pn time averaged spectrum for each

¹After removal of the time intervals affected by high flaring background.

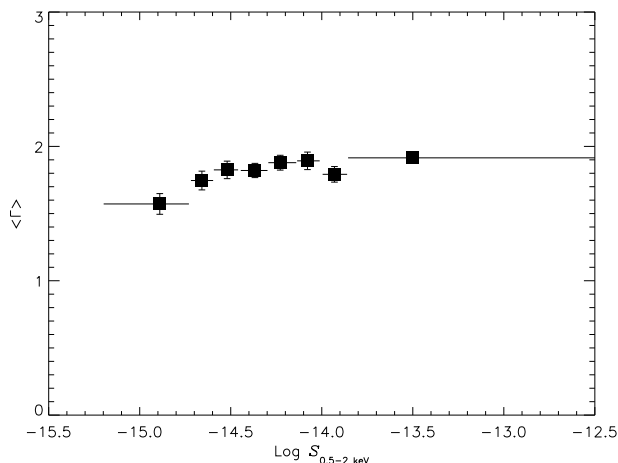


Figure 1. Dependence of $\langle \Gamma \rangle$ on 0.5-2 keV flux. For each source we used the values of Γ from its best fit model.

object. Due to the different instrumental responses of the detectors we did not combined MOS and pn data. Spectra were extracted in the energy interval from 0.2 to 12 keV where the *XMM-Newton* instruments are best calibrated. In order to use χ^2 minimisation to find the best fit model for each object we grouped the spectra with a minimum of 30 counts per bin.

We have obtained the best fit model for each source individually using the *xspec* 11.3.0 package. MOS and pn spectra were fitted simultaneously with the same model and spectral parameters. We used the F-test to measure the significance of detection of each individual component. We selected a confidence level threshold of 95% to accept an additional spectral component as being real. We started the spectral fitting using a model consisting of an absorbed power law, with an absorption component fixed to the Galactic column density in the direction of the *Lockman Hole*, $N_{\text{H}} = 5.7 \times 10^{19} \text{ cm}^{-2}$, and a second absorption component that was left free to vary. For sources with detected soft excess emission we fitted this component with a black body model. In some cases the black body model was not able to reproduce the spectral signatures of the soft excess emission. For these sources acceptable fits were obtained using a partial covering model. Signatures of $\text{FeK}\alpha$ emission were detected in eight sources. In all cases a Gaussian model provided an acceptable fit to the data.

In this proceeding we will show the properties of the broad band continuum shape and X-ray absorption of our sources. A more detailed description of the results of our spectral analysis can be found in Mateos (2005).

3.1. Broad band continuum shape

The mean spectral slope of our sources was found to be $\langle \Gamma \rangle = 1.87 \pm 0.02$. Using the values of Γ from the best fit model of each object we did not see any clear dependence of $\langle \Gamma \rangle$ on the 0.5-2 keV flux as it is shown in Figure 1. We

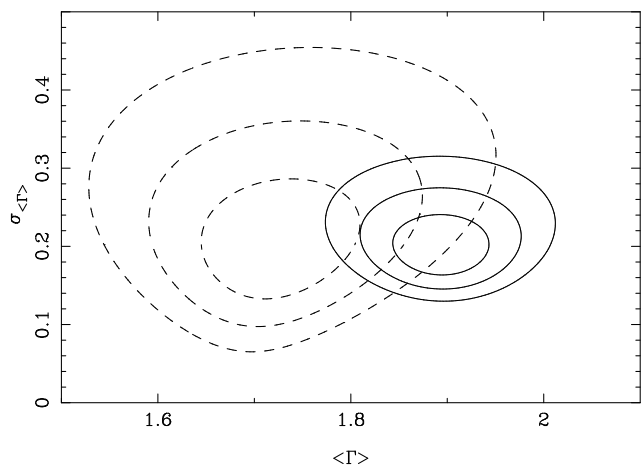


Figure 2. Confidence intervals for the mean spectral slope $\langle \Gamma \rangle$ and intrinsic dispersion $\sigma_{\langle \Gamma \rangle}$ for our samples of type-1 (solid lines) and type-2 (dashed lines) AGN from the maximum likelihood analysis. The three contours correspond to 1, 2 and 3σ for two interesting parameters (i.e. $\Delta\chi^2 = 2.3, 6.17$ and 11.8).

found the mean continuum shape to be $\langle \Gamma \rangle = 1.89 \pm 0.03$ for type-1 AGN and $\langle \Gamma \rangle = 1.71 \pm 0.03$ for type-2 AGN, although with a significant dispersion in the individual values in both samples of objects. Assuming a Gaussian distribution of spectral slopes we used the maximum likelihood method of Maccacaro (1988) to calculate the mean continuum shape and its intrinsic dispersion. The results of this analysis are shown in Table 1. In Figure 2 we show the maximum likelihood confidence intervals of $\langle \Gamma \rangle$ and $\sigma_{\langle \Gamma \rangle}$ for type-1 and type-2 AGN. Although our results suggest that type-2 AGN tend to have on average flatter spectral slopes than type-1 AGN we found the significance of this effect to be only of 1.62σ .

Table 1. Mean spectral photon index obtained with the Maximum Likelihood analysis and with the standard weighted mean. The spectral slopes from the sources' best fit model were used.

Sample	Maximum Likelihood		Weighted Mean
	$\langle \Gamma \rangle$	$\sigma_{\langle \Gamma \rangle}$	
Whole sample	$1.92^{0.03}_{0.18}$	$0.28^{0.04}_{0.13}$	1.87 ± 0.02
type - 1 AGN	$1.89^{0.06}_{0.05}$	$0.20^{0.04}_{0.04}$	1.89 ± 0.03
type - 2 AGN	$1.72^{0.10}_{0.08}$	$0.20^{0.10}_{0.07}$	1.71 ± 0.03

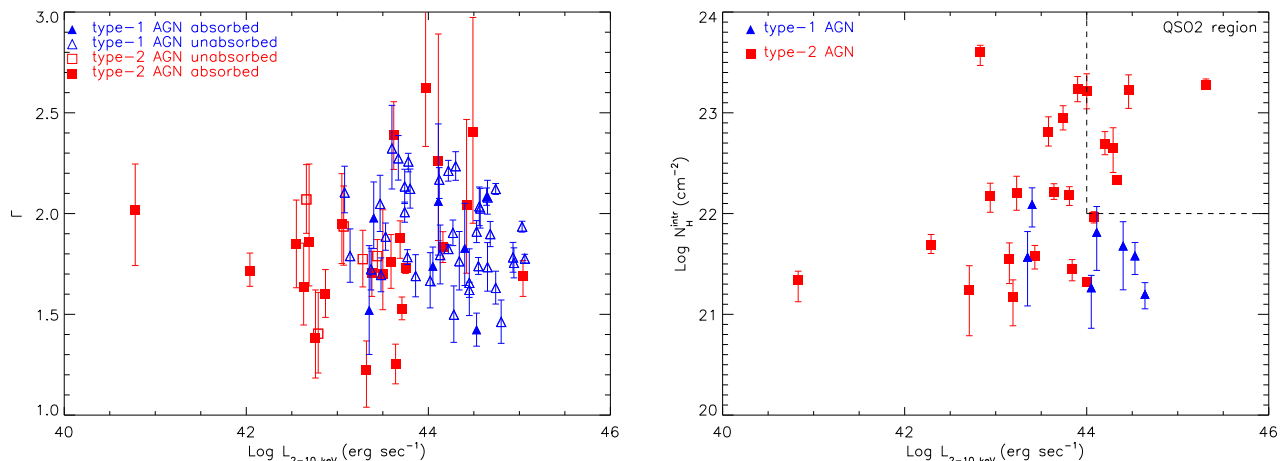


Figure 4. Dependence of Γ (left) and $N_{\text{H}}^{\text{intr}}$ (right) on 2-10 keV (rest-frame) luminosity. Error bars correspond to 90% confidence.

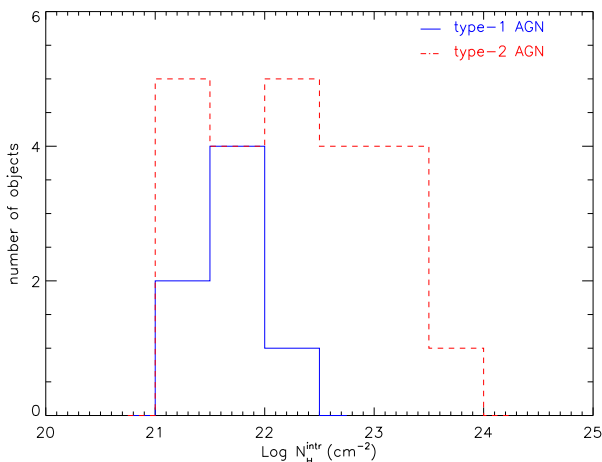


Figure 3. Distributions of intrinsic (rest-frame) absorbing column densities for type-1 and type-2 AGN.

3.2. X-ray absorption

We detected X-ray absorption (F-test $\geq 95\%$) in $\sim 38\%$ of our sources, including $\sim 10\%$ of type-1 AGN and $\sim 77\%$ of type-2 AGN². We found the fractions of absorbed sources among type-1 and type-2 AGN to be different with a significance of $\geq 99.99\%$. The distributions of measured intrinsic (rest-frame) column densities for absorbed type-1 and type-2 AGN are shown in Figure 3. The absorbing column densities for type-1 AGN were found to be in a narrow range from $10^{21} - 10^{22} \text{ cm}^{-2}$. The distribution of $N_{\text{H}}^{\text{intr}}$ for type-2 AGN covers a much broad range of values with a significant number of sources having $N_{\text{H}}^{\text{intr}} \geq 10^{23} \text{ cm}^{-2}$.

²The values for the fractions of absorbed sources have been corrected for the expected spurious detections.

3.3. Dependence of AGN X-ray properties on luminosity and redshift

In Figures 4 and 5 we show the dependence of the photon index and intrinsic absorption on 2-10 keV (rest-frame) luminosity and redshift for our samples of type-1 and type-2 AGN. We did not find a clear dependence of the X-ray spectral properties of our AGN on X-ray luminosity. A basic Spearman Rank correlation test of Γ and $N_{\text{H}}^{\text{intr}}$ versus redshift for type-1 AGN implies that there is not correlation between these parameters. This lack of correlation of Γ -redshift was also found for type-2 AGN. The observed deficit of high redshift AGN with low $N_{\text{H}}^{\text{intr}}$ is probably due to a selection effect, since it is easier to detect highly absorbed sources at high redshifts.

4. VARIABILITY ANALYSIS

The previous results were obtained by the analysis of the time averaged spectrum of each individual source. However we know AGN are strongly variable sources, showing their fastest variability in X-rays. X-ray variability studies are a good complement to spectral analyses as they can provide valuable information about the nature and structure of the innermost regions in AGN where the X-rays are emitted.

4.1. Flux variability

To study X-ray flux variability we built light curves for our sources using the 0.2-12 keV count rates detected on each individual observation. An example of a typical light curve is shown in Figure 6. For this analysis we have used only pn data because in general pn count rates are better constraint than MOS count rates. We have pn light curves available (with at least two points) for 120

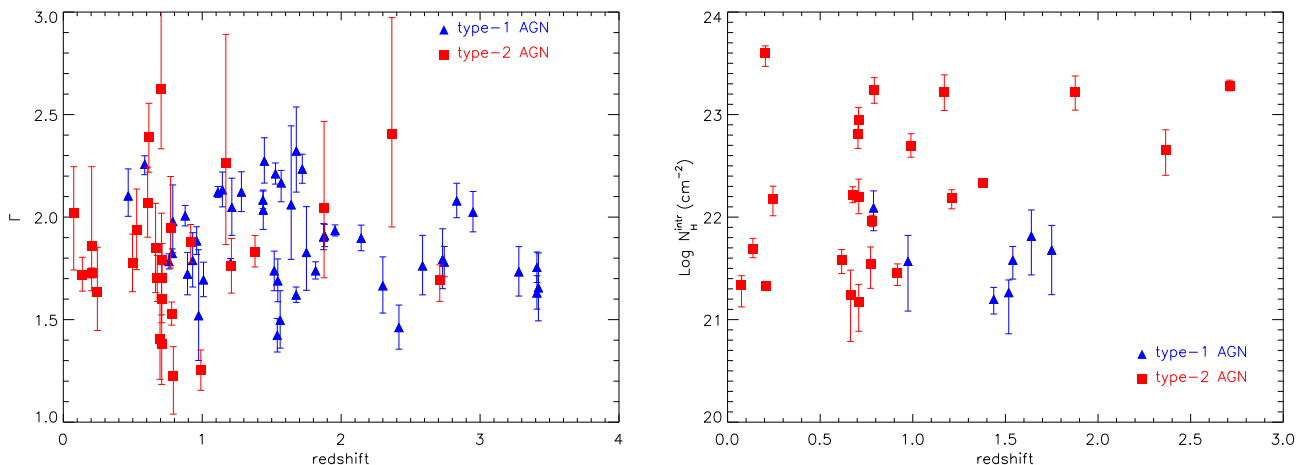


Figure 5. Dependence of Γ (left) and $N_{\text{H}}^{\text{intr}}$ (right) on redshift. Error bars correspond to 90% confidence.

out of the 123 objects in our sample including 45 type-1 AGN and 27 type-2 AGN. To search for sources with flux variability we have used the χ^2 test³, where χ^2 is defined as

$$\chi^2 = \sum_i \frac{(x_i - \langle x \rangle)^2}{\sigma_i^2} \quad (1)$$

x_i are the 0.2-12 keV count rates from each individual observation, N is the number of points in the light curve, $\langle x \rangle$ is the mean count rate and σ_i are the errors in the count rates x_i . We selected a 3σ confidence threshold for detection of variability. The results of the χ^2 test are summarised in Table 2, where the fractions of sources with detected variability have been corrected for the expected spurious detections. Flux variability was detected in $\sim 50\%$ of the sources in our sample. We compared the fractions of sources with detected flux variability among type-1 and type-2 AGN and we found the significance of them of being different of only 75%. The fraction of sources variable in flux for unidentified objects is significantly lower than for AGN. Most unidentified objects are among the faintest sources in our sample, and therefore their light curves have lower S/N which makes for difficult the detection of variability.

To quantify the amplitude of flux variability in our sources we have used the *excess variance*, σ_Q , that we have calculated using the method developed by Almaini (2000). This method is the most appropriate in the regime of gaussian statistics and for light curves with points having different measurement errors. The *excess variance* gives us the fraction of the total flux that is variable and therefore we can compare the values obtained for sources with different count rates. The distribution of measured values of σ_Q in shown in Figure 7 for the whole sample of sources (solid histogram) and for the objects with detected flux variability from the χ^2 test (filled histogram).

³We checked that using the count rates from the 0.2-12 keV energy band all sources have more than 10 counts (background subtracted) on each point of their light curves and therefore we can assume gaussian statistics during the analysis.

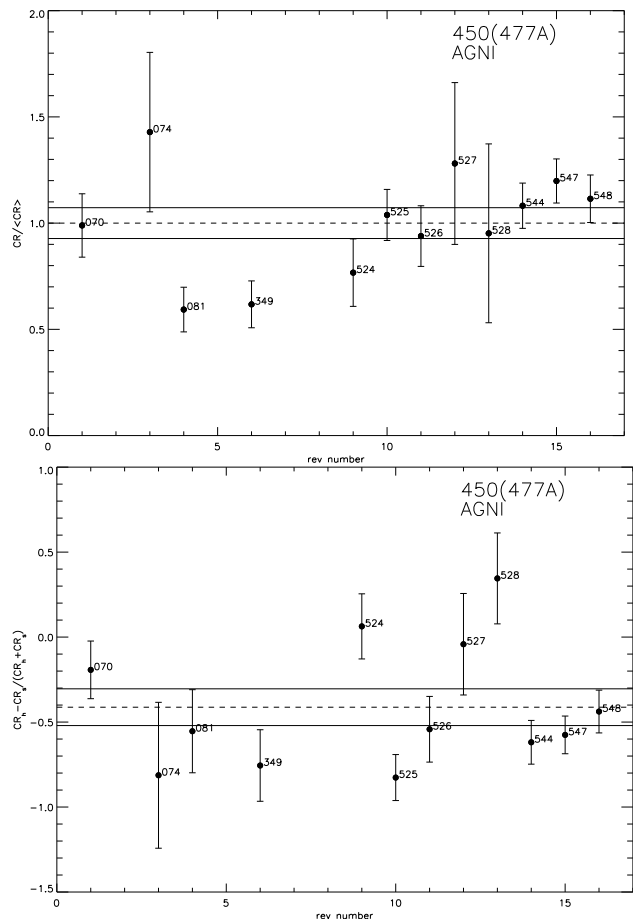


Figure 6. Typical light curves of a source with detected flux (top) and spectral variability (bottom). Each point represents the data from an individual observation and is labelled with the revolution number for that observation. The distribution of points is not uniform in time and can vary from days to years.

Table 2. Fractions of sources with detected flux and spectral variability from the χ^2 test.

Group (1)	N_{tot} (2)	n_{flux} (3)	$f_{\text{flux}}(\%)$ (4)	n_{sp} (5)	$f_{\text{sp}}(\%)$ (6)
All	120	62	51 ± 7	24	20 ± 6
type-1 AGN	45	31	68 ± 11	6	14 ± 8
type-2 AGN	27	13	48 ± 15	9	34 ± 14
Unidentified	48	18	37 ± 11	9	19 ± 9

Columns are as follows: (1) Group of sources; (2) Number of objects in the group; (3) Number of sources with detected flux variability (confidence $\geq 3\sigma$); (4) Fraction (corrected for spurious detections) of sources with detected flux variability; (5) Number of sources with detected spectral variability (confidence $\geq 3\sigma$); (6) Fraction (corrected for spurious detections) of sources with detected spectral variability; Errors are 90% intervals.

We have detect a broad range of flux variability amplitudes going from ~ 0.1 to ~ 0.65 . We see in Figure 7 that the efficiency of detection of flux variability depends strongly on the amplitude of the variability, specially for values of σ_Q lower than ~ 0.3 . The mean amplitude of flux variability (including objects with no detected variability from the χ^2 test) was found to be 0.22 for the whole sample of sources, 0.27 ± 0.02 for type-1 AGN and 0.21 ± 0.03 for type-2 AGN.

As it is shown in Figure 8 no dependence of the mean amplitude of flux variability on luminosity and redshift was seen for our identified sources.

4.2. Spectral variability

Most of the sources in our sample are too faint to conduct a detailed spectral analysis of their emission properties on each individual observation, as the uncertainties in the spectral parameters will be very large to detect small changes in the spectral shape. Therefore to search for spectral variability in our sources we have used a broad band hardness ratio HR, that we defined as

$$HR = \frac{CR_h - CR_s}{CR_h + CR_s} \quad (2)$$

where CR_h and CR_s are the 0.5-2 and 2-12 keV count rates of the sources from each observation. To search for sources with spectral variability we have compared the mean HR of each source to the ones measured for each individual observation using χ^2 test (as for flux variability). We detected spectral variability in $\sim 20\%$ of the objects in our sample including $\sim 14\%$ of type-1 AGN and $\sim 34\%$ of type-2 AGN. We found that the fractions of

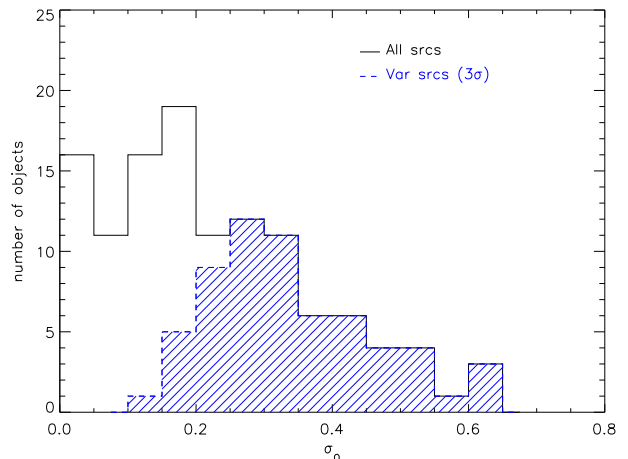


Figure 7. Distribution of measured amplitudes of flux variability for the whole sample of objects (solid histogram) and for the sources where we detected flux variability with the χ^2 test with a confidence level $\geq 3\sigma$.

objects with spectral variability among type-1 and type-2 AGN are different with a significance of 99%, i.e. spectral variability seems to be more common in type-2 AGN.

4.3. Fractions of variable sources

Our variability analysis has shown that $\sim 50\%$ of the sources in our sample are variable in flux and $\sim 20\%$ in spectral shape. We have studied whether the efficiency of detection of variability depends on the signal to noise of our data. In Figure 9 we show the fraction of sources with detected flux and spectral variability as a function of the mean 0.2-12 keV count rate (top) and as a function of the error in the mean HR (bottom). We see that the fractions of sources with detected spectral and flux variability strongly depend on the S/N of the data. Our results show that the fraction of sources in our sample with flux variability could be $\geq 80\%$ while the fraction of objects with spectral variability could be $\geq 50\%$.

5. DISCUSSION

We have investigated the X-ray spectral and variability properties of the 123 brightest sources detected with *XMM-Newton* in the *Lockman Hole* field. Using for each source the results from its best fit model we have been able to explain the observed hardening of the mean photon index with X-ray flux as an increase in X-ray absorption at faint fluxes. We found the mean 0.2-12 keV photon index to be ~ 1.9 for the whole sample of objects and for type-1 AGN, and ~ 1.7 for type-2 AGN. We found a scatter of best fit photon indices of ~ 0.28 for the whole sample of sources and of ~ 0.2 for the subsamples of type-1 and type-2 AGN. This scatter in Γ is intrinsic and not related to X-ray absorption. Significant X-ray absorption was detected in $\sim 37\%$ of the objects in our sample

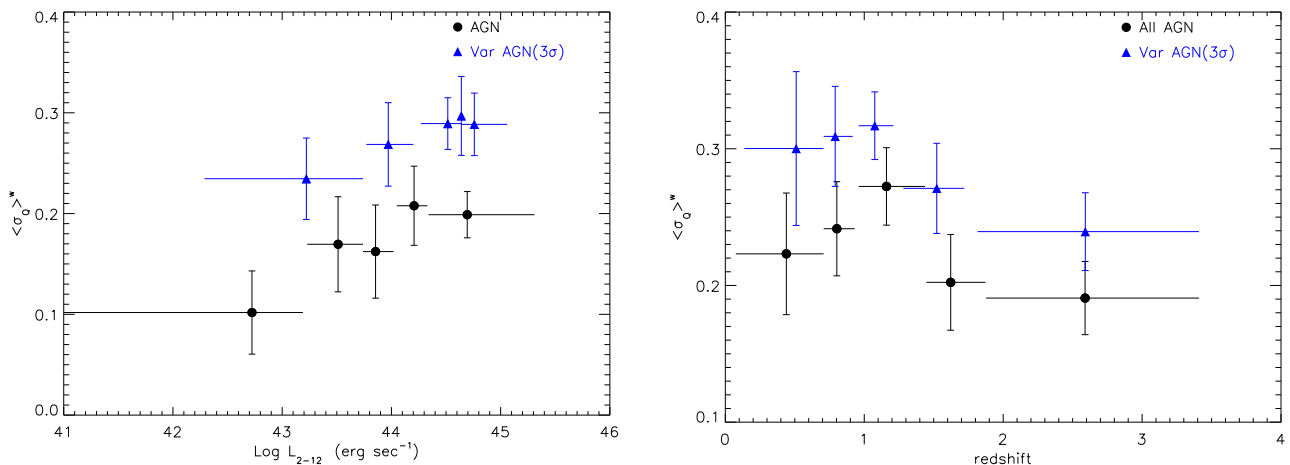


Figure 8. Dependence of the mean amplitude of flux variability (weighted mean) on 2-10 keV luminosity (left) and redshift (right) for all AGN and for the objects with detected flux variability from the χ^2 test.

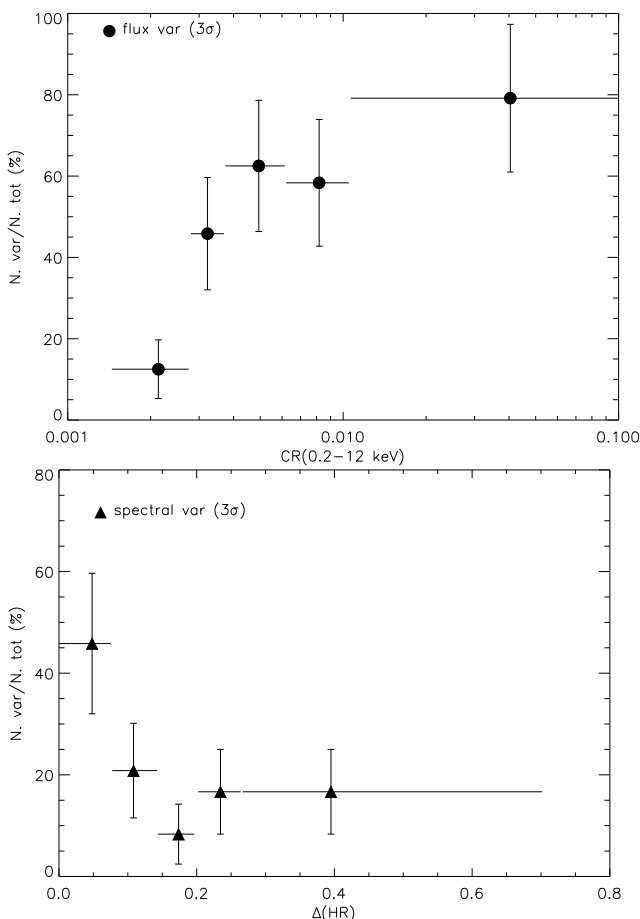


Figure 9. Top: Fraction of sources with detected flux variability as a function of the mean 0.2-12 keV count rate. Bottom: Fraction of sources with detected spectral variability as a function of the error in the mean HR.

including $\sim 10\%$ of type-1 AGN and $\sim 77\%$ of type-2 AGN. In terms of the standard unified model of AGN X-ray absorption and optical obscuration should be correlated. The results of our analysis show that this does not hold for a significant fraction of type-1 and type-2 AGN in our sample. We did not find evidences of spectral dependence of the AGN in our sample on X-ray luminosity and redshift.

A fraction of $\sim 50\%$ of the sources in our sample were found to vary with flux on long time scales. However using only the data with best signal to noise this fraction increases up to 80%, implying that flux variability is a common property of AGN. The mean amplitude of flux variability was found to be ~ 0.22 . The number of sources with detected spectral variability is $\sim 20\%$ but using only the data with best signal to noise the fraction increases up to $\sim 50\%$. Spectral variability seems to be less common than flux variability in our sources, however we need to note that spectral variability is more difficult to detect than flux variability. The fractions of sources with detected flux variability do not differ significantly among type-1 and type-2 AGN, however we found spectral variability to be more common in type-2 AGN with a significance of 99%. We did not find the variability properties of the AGN in our sample to depend on the luminosity or redshift of the objects.

REFERENCES

- Maccaro, T., Gioia, I. M., Wolter, A., et al. 1988, ApJ, 326, 680
- Almaini, O., Lawrence, A., Shanks, T., et al. 2000, MNRAS, 315, 325
- Mateos, S., Barcons, X., Carrera, F. J., et al. 2005, A&A accepted (astro-ph/0506718)